AREA PRODUCTION IN SUPERCRITICAL, TRANSITIONAL MIXING LAYERS FOR REACTIVE FLOW APPLICATIONS

N. Okong'o and J. Bellan†

Jet Propulsion Laboratory, California Institute of Technology, Pasadena, CA. 91109

†Corresponding author: Dr. J. Bellan

Jet Propulsion Laboratory

California Institute of Technology

MS. 125-109

4800 Oak Grove Drive

Pasadena, CA 91109

USA

Tel: (818) 354-6959

Fax: (818) 393-5011

e-mail: Josette.Bellan@jpl.nasa.gov

Word Count: Abstract: 291; Paper: 5403 (Introduction 287; Model 429; Results 424+571+339; Conclusions 562; Ackn 115; Eqs 301; Refs 175; Tables and figures 2200).

Colloquium on Turbulent Combustion

(Turbulent Non-Premixed Flames)

Oral presentation

ABSTRACT

An investigation of surface area production is conducted for supercritical mixing layers; the results are relevant to flame area evolution and fluid disintegration. In this study, the surface is chosen perpendicular to the mass fraction gradient. Employing a database of transitional states obtained from Direct Numerical Simulation of temporal three-dimensional supercritical mixing layers for two binary-fluid systems, it is shown that independent of the initial perturbation wavelength used to excite the layer, area production is primarily determined by strain rather than compressibility. Thus, the conservation equation for the strain-rate/conserved-scalar-gradient tensorial product is derived for real, non-ideal fluids, and the contributions to its evolution are identified and evaluated. The results show that, independent of the species system and perturbation wavelength, strain and convective effects always produce area, whereas species mass flux and rotational effects always destroy it. Viscosity effects are negligible, and the pressure gradient effect generally destroys area. A large pressure-gradient-term contribution to the strain-rate/conserved-scalar-gradient RMS is found, and is attributed to departures from perfect-gas behavior. Area production increases with decreasing initial density stratification of the layer, and with smaller perturbation wavelengths. The most active layer also exhibits the largest probability of having perpendicular vorticity and conserved-scalar-gradient vectors. To elucidate the significance of this aspect, a conservation equation for the vorticity/conserved-scalar-gradient is derived and its budget is examined. On a local cross-stream basis, the vorticity/conserved-scalar-gradient scalar product evolution is shown to be governed by the species mass flux and the viscous stress, while on a volumetric basis, compressibility is the sole contributor; as a consequence of the volumetric equation, a time invariant of the system is identified. It is also shown that the dilatation acts as a 'restoring force', always inducing changes towards the maximum area creation.

1 Introduction

Flame behavior is notoriously affected by the interactions of the strain rate, S_{ij}, and vorticity, ω, with scalar fields [1]. These interactions can be conceptualized as a stretch of the flame surface due to strain, and as a folding and wrapping of this stretched surface due to the action of ω. These processes must coexist in order to conserve and/or promote the development of flame surface area. Flame stretching has been studied extensively [2], [3], [4], and the alignment of ω and the scalar gradient, ζ, with S_{ij} have also been investigated [5]; all these studies addressed subcritical fluid conditions. Conceptually, when ω and ζ are orthogonal, flames become wrapped around a vortex tube, thereby increasing the surface area [1]. However, when ω and ζ are parallel, transport of reactants increase within the flame, and no increase in flame area occurs [1]. More generally, it is of interest to inquire about the mechanisms leading to changes in a surface area (e.g. relevant to fluid disintegration for combustion enhancement) due to turbulence; an evaluation of these mechanisms in the absence of chemical reaction leads to a conservative estimate of these effects, with implications for reacting situations. The supercritical regime is chosen herein because of the numerous combustion systems, such as liquid rocket, gas turbine and diesel engines that operate at supercritical pressures with respect to the fuel.

Despite the wide range of combustion applications, there is only a scant body of fundamental studies on shear-induced turbulence under supercritical conditions [6], [7]; even less is known about aspects of supercritical turbulence relevant to reacting flows [6], [8], [9], [10]. The present investigation represents a step in elucidating some of these aspects. As detailed in [11], a thermodynamic state will here be called 'supercritical' if either the thermodynamic pressure, p, or the temperature, T, exceeds its critical value, p_c, or T_c, respectively, i.e. $p_r \equiv p/p_c > 1$ or $T_r \equiv T/T_c > 1$ for the fuel.

2 Conservation equations and surface creation

The present governing equations originate in a model previously validated [12] with an entire set of micro-gravity drop-data [13], encompassing the C_7H_{16}/N_2 subcritical and supercritical regimes. This model was adapted for mixing layers [14], and implemented [6] to achieve transitional mixing states. The governing equations are succinctly stated below. Due to space restrictions, the published model equations will not be reproduced here except for those that are essential to the present derivation.

Using the classical nomenclature for mixing layer coordinates (x_1 streamwise, x_2 cross-stream, x_3 spanwise), the conservation equations for a binary mixture of general (Newtonian) fluids are:

$$\partial\rho/\partial t + \partial\left[\rho u_j\right]/\partial x_j = 0, \tag{1}$$

$$\partial\left(\rho u_i\right)/\partial t + \partial\left[\rho u_i u_j + p\delta_{ij} - \tau_{ij}\right]/\partial x_j = 0, \tag{2}$$

$$\partial\left(\rho e_t\right)/\partial t + \partial\left[\left(\rho e_t + p\right)u_j - u_i\tau_{ij} + q_{IK,j}\right]/\partial x_j = 0, \tag{3}$$

$$\partial\left(\rho Y_2\right)/\partial t + \partial\left[\rho Y_2\ u_j + j_{2j}\right]/\partial x_j = 0, \tag{4}$$

where ρ is the density, $e_t = e + u_i u_i/2$ is the total energy (i.e. internal energy, e, plus kinetic energy) and Y_2 is the mass fraction of the lower-stream ($x_2 < 0$) heavier fluid ($Y_1 = 1 - Y_2$). Furthermore, $\mathbf{q}_{IK}$ is the Irwing-Kirkwood (subscript IK) form of the heat flux vector [15], $\mathbf{j}_2$ is the species mass flux vector and τ_{ij} is the Newtonian viscous stress tensor

$$\tau_{ij} = \mu\left[2S_{ij} - (2/3)S_{kk}\delta_{ij}\right], \quad S_{ij} = (1/2)(\partial u_i/\partial x_j + \partial u_j/\partial x_i), \tag{5}$$

where δ_{ij} is the Kronecker delta function and μ is the mixture viscosity. According to [12], the form of the diffusional fluxes is:

$$q_{IK,j} = -\left[\lambda'_{IK}\partial T/\partial x_j + \alpha_{IK}R_u T[m/(m_1 m_2)]j'_{2j}\right], \tag{6}$$

$$j_{2j} = -\left[j'_{2j} + \alpha_{BK}Y_1Y_2\ (\rho D/T)\ \partial T/\partial x_j\right], \tag{7}$$

$$j'_{2j} = \rho D\left[\alpha_D\partial Y_2/\partial x_j + Y_1Y_2 m_1 m_2/(R_u T m)\left(v_{,2}/m_2 - v_{,1}/m_1\right)\partial p/\partial x_j\right] \tag{8}$$

where eq. 6 is the IK form of the heat flux ([15]); D is the binary diffusion coefficient; the mole fraction is $X_\alpha = m_\alpha Y_\alpha/m$; m_α is the molar weight of pure species α; the mixture molar weight is $m = X_1 m_1 + X_2 m_2$; the molar volume is $v = m/\rho$; $v_{,\alpha}$ is the partial molar volume; α_D is the mass diffusion factor; and λ'_{IK} is a thermal conductivity. Also, α_{IK} and α_{BK} are the thermal diffusion factors corresponding to the IK and the Bearman-Kirkwood (subscript BK) forms of the heat flux ([15]), respectively; they are the transport coefficients associated with the Soret (in the molar fluxes) and the Dufour (in the heat flux) terms of the transport matrix, and are characteristic functions of (p, T, Y_i) for each particular species pair. Although $\alpha_{IK}(p, T, Y_i)$ and $\alpha_{BK}(p, T, Y_i)$ are currently unknown, it has been shown [12] that

$$\alpha_{IK} = \alpha_{BK} + (1/R_u T)(m_1 m_2/m)(h_{,2}/m_2 - h_{,1}/m_1) \tag{9}$$

where $h_{,\alpha}$ is the partial molar enthalpy. Here, $\lambda'_{IK} = \lambda + X_1 X_2\ \alpha_{IK}\ \alpha_{BK} R_u \rho D/m$, where λ is the thermal conductivity. To calculate $\alpha_D = 1 + X_\alpha[\partial \ln(\varphi_\alpha)/\partial X_\alpha]$, the fugacity coefficients, φ_α, are calculated from the equation of state (EOS); α_D measures departures from fluid mixture ideality (i.e. from $\alpha_D = 1$) [12]. The Peng-Robinson EOS is employed in conjunction with the above equations [14]. The Schmidt number, $Sc = \mu/(\rho \alpha_D D)$, and the Prandtl number, $\mathrm{Pr} = \mu C_p/(m\lambda)$, are correlated at fixed pressures as functions of (T, Y_i) to mimic the accurate values obtained in calculations based on the exact values of D and λ [10], [14], [16]. A reference μ, μ_R, is obtained from the specified initial Reynolds number, $\mathrm{Re}_0 = 0.5(\rho_1 + \rho_2)\Delta U_0 \delta_{\omega,0}/\mu_R$ where $\Delta U_0 = U_1 - U_2$ is the initial velocity difference across the mixing layer, which is calculated from the specified value of the initial Mach number, M_0, and $\delta_{\omega,0}$ is the initial vorticity thickness [14]; μ_R is further used to calculate $\mu(T)$ [6], [14].

In a coordinate system fixed to a surface oriented perpendicular to ζ, its stretch is [4]

$$(1/A)(dA/dt) = -(\zeta_i \zeta_j S_{ij})/(\zeta_k \zeta_k) + S_{kk}, \tag{10}$$

where A is the area of the surface, such as an infinitesimally thin flame. This study presents an examination of the phenomena responsible for the variation of $(1/A)(dA/dt)$.

3 Results and Discussion

To understand the phenomena contributing to $(1/A)(dA/dt)$, a transitional state database obtained from Direct Numerical Simulation (DNS) of three-dimensional (3D) supercritical temporal mixing layers [6], [9], [10] is analyzed. Streamwise and spanwise perturbations of wavelengths λ_1 and λ_3 and amplitudes F_{2D} and F_{3D} are imposed on the initial velocity profile in order to excite the layer and eventually lead to transition [6]. Following typical temporal simulation protocols [17], the computational domain size is $4\lambda_1$ and $4\lambda_3$ in the x_1 and x_3 directions, and the evolution of the layer encompasses rollup and two pairings. Information relevant to the initial conditions is listed in Table 1. The initial velocity profile, the form of the forcing perturbations and the boundary conditions are all discussed in detail in [6], [7] and [14]. Consistent with the validated results in [12], $\alpha_{IK} = 0.1$ for C_7H_{16}/N_2, and $\alpha_{BK} = 0.2$ for O_2/H_2 as in [16] and [10]. The O_2/H_2 mixture is potentially reactive, whereas the C_7H_{16}/N_2 is not; however, preliminary evidence [18] indicates that the addition of O_2 to N_2 affects only minimally the distribution of the conserved scalar, which in this non-reactive situation is that of the species mass fraction (i.e. $\zeta = \nabla Y_2$).

An examination of the braid and between-the-braid contours of $(1/A)(dA/dt)$ (not shown) reveals that much of the activity is spatially concentrated at the edge of the coherent vortices, with substantial contribution from the interior of the mixing layer; thus, both large and small scales contribute to $(1/A)(dA/dt)$, which exhibits both positive and negative local regions. To quantify the area creation, displayed in Fig. 1 are the average (1a) and RMS (1b), of $(1/A)(dA/dt)$ for the four layers. Clearly the $(1/A)(dA/dt)$ average is overwhelmingly positive. Most area creation occurs inside the layers and on the lighter fluid side, and the C_7H_{16}/N_2 (HN) layers create more area than the O_2/H_2 (OH) layers, meaning that a smaller initial density stratification produces more area. Also, area production seems uncorrelated with the magnitude of Re_m (see Table 1). Noteworthy, layers perturbed with a smaller λ_1 create more area, independent of the species system; this finding represents a first step towards area production control in turbulent supercritical fluids. The relative magnitude of the RMS is similar to that for the average, indicating that larger area production is accompanied by a wider range of activity. Because both compressibility and strain contribute to $(1/A)(dA/dt)$, braid and between-the-braid contours of $[(-\zeta_i\zeta_j S_{ij})\,/(\zeta_k\zeta_k)](\delta_{\omega,0}/\Delta U_0)$ and $S_{kk}(\delta_{\omega,0}/\Delta U_0)$ were compared (not shown), revealing that the range of the latter term is smaller by as much as a factor of 4 than that of the first term. Further, the budget of eq. 10 is illustrated in Fig. 2 for the HN800 layer; the displayed average is typical for all layers, and the RMSs (not shown) exhibit a similar result. These results show that strain contributes substantially more than compressibility to area production, motivating its further examination.

3.1 Conservation equation for the strain-rate/mass-fraction-gradients product

To inquire about the processes contributing to the evolution of $(-\zeta_i\zeta_j S_{ij})$, we obtained the following equation:

$$\begin{aligned}\frac{D}{Dt}\left(-\zeta_i\zeta_j S_{ij}\right) &= 2\frac{\partial u_k}{\partial x_i}\zeta_j\zeta_k S_{ij} + S_{ik}S_{kj}\zeta_i\zeta_j + \frac{1}{4}\left(\omega_i\zeta_i\omega_j\zeta_j - \omega_i\omega_i\zeta_j\zeta_j\right) + \zeta_i\zeta_j\frac{\partial}{\partial x_i}\left(\frac{1}{\rho}\frac{\partial p}{\partial x_j}\right) + \\ &\quad 2\zeta_i S_{ij}\frac{\partial}{\partial x_j}\left(\frac{1}{\rho}\frac{\partial j_{2k}}{\partial x_k}\right) - \zeta_i\zeta_j\frac{\partial}{\partial x_i}\left(\frac{1}{\rho}\frac{\partial \tau_{jk}}{\partial x_k}\right). \qquad (11)\end{aligned}$$

The first term in eq. 11 originates from the convection term in the ζ equations, the second and third terms portray strain and rotational effects, the fourth term reflects the ∇p influence in the momentum equation, the fifth term is due to species mass diffusion and the last term represents viscous effects. Noteworthy,

$(-\zeta_i\zeta_j S_{ij})$ is also the source term of $(\zeta_k\zeta_k)$ (see eq. 10) since

$$\frac{1}{2}\frac{D(\zeta_k\zeta_k)}{Dt} = -\zeta_i\zeta_j S_{ij} - \zeta_i\frac{\partial}{\partial x_i}\left(\frac{1}{\rho}\frac{\partial j_{2j}}{\partial x_j}\right). \tag{12}$$

Examination of braid and between-the braid $\left(-\zeta_i\zeta_j S_{ij}\right)$ contour plots (not shown) revealed that the activity is locally very concentrated and occurs within the high density gradient magnitude (HDGM) regions identified in supercritical mixing layers for various species systems [6], [9], [10]. However, not all HDGM regions exhibit high $\left(-\zeta_i\zeta_j S_{ij}\right)$ activity. This indicates that only some of the processes responsible for HDGM formation discussed in [10] can activate $\left(-\zeta_i\zeta_j S_{ij}\right)$.

To identify the phenomena responsible for the $\left(-\zeta_i\zeta_j S_{ij}\right)$ activity, illustrated in Fig. 3 are the average (3a) and RMS (3b) of the terms in eq. 11 for the HN800 layer. Most of the activity occurs on the N_2 side of the layer, where the lighter fluid resides. For the average, strain and convection effects lead to production of area, whereas rotational and species mass flux effects destroy it; since the surface is oriented perpendicular to $\boldsymbol{\zeta}$, the species mass flux tends to decrease $\boldsymbol{\zeta}$, explaining the decrease in A. ∇p can either destroy surface area, or produce it near the N_2 freestream; the viscous effect is negligible. Strain and convection have similar magnitudes at the same location where rotation matches the species mass flux, whereas elsewhere within the layer strain and rotation dominate; ∇p has the smallest contribution. Most of the RMS is however dominated by the ∇p term, while the other contributions, with the exception of the much smaller viscous term, are equivalent. The results for the HN500 layer are similar, with the exception that the ∇p term only destroys surface area and its contribution to the RMS, while still being the most significant, is closely followed by that of the other terms. Equivalent plots to those of Fig. 3 are displayed in Fig. 4 for the OH750 layer; these plots are typical of the OH550 layer as well. Compared to the HN layers, the average (Fig. 4a) and RMS (Fig. 4b) are here one and two orders of magnitude smaller, respectively, indicating a more subdued activity. In contrast to the HN layers, there is a much clearer separation in the average between the dominating aspect of strain rate in producing surface area compared to convective effects, and that of rotation with respect to the mass flux in destroying surface area. Also in contrast to the HN layers, the ∇p effects are small in the RMS, with only viscosity being smaller. Superimposing braid and between-the-braid contour plots of $\mid \nabla\rho \mid$, $\mid \nabla p \mid$ and $\boldsymbol{\zeta}\boldsymbol{\zeta}\nabla(\nabla p/\rho)$ led to the conclusion that whereas in the HN layers the regions of $\boldsymbol{\zeta}\boldsymbol{\zeta}\nabla(\nabla p/\rho)$ activity coincided with the overlap of the significant $\mid \nabla p \mid$ with the HDGM regions, no such behavior existed for the OH layers. Considering that for the (p,T) conditions of the OH layers both fluids

are virtually perfect gases [10], whereas strong departures from perfect gas behavior are exhibited by the HN layers [6], [14], the large contribution of $\zeta\zeta\nabla(\nabla p/\rho)$ to the $(-\zeta_i\zeta_j S_{ij})$ RMS is attributed to the strong p coupling with ρ through the real gas EOS.

Volume averages of $[D\left(-\zeta_i\zeta_j S_{ij}\right)/Dt]\delta^4_{\omega,0}/\Delta U_0^2$ yield -1.94×10^{-5}, 7.69×10^{-3}, 2.24×10^{-5} and -1.73×10^{-5} for the HN500, HN800, OH750 and OH550 layers, indicating, consistent with the $(1/A)(dA/dt)$ results, that most of the activity occurs within the HN800 layer. To understand the more considerable $(-\zeta_i\zeta_j S_{ij})$ activity of the HN800 layer, we analyzed the vorticity/mass-fraction-gradient scalar product.

3.2 Vorticity/mass-fraction-gradient scalar product

Because the alignment of $\boldsymbol{\omega}$ and $\boldsymbol{\zeta}$ influences the area production, the PDF of $\cos(\boldsymbol{\omega},\boldsymbol{\zeta})$ is shown in Fig. 5; the range of Y_2 used in the calculation follows the provisional O_2/H_2 flammability limits of $Y_2 = 0.4113$ and $Y_2 = 0.9895$ of the rich and lean limits [19] for the OH layers, and encompasses the entire range of Y_2 values inside the HN layer. Similar to the findings of [1] for subcritical turbulent conditions, the PDF exhibits a maximum for $\cos(\boldsymbol{\omega},\boldsymbol{\zeta})$ =0, i.e. for the vectors being perpendicular. All PDFs have a similar peak magnitude, with the exception of the HN800 layer whose peak is considerably higher, consistent with the larger activity in area production found from Fig. 3 and the budget of $(-\zeta_i\zeta_j S_{ij})$.

To examine the phenomena determining the value of $\cos(\boldsymbol{\omega},\boldsymbol{\zeta})$, the conservation equation for $(\boldsymbol{\omega}\cdot\boldsymbol{\zeta})$ was derived

$$\frac{D}{Dt}(\boldsymbol{\omega}\cdot\boldsymbol{\zeta}) = -(\boldsymbol{\omega}\cdot\boldsymbol{\zeta})(\nabla\cdot\mathbf{u}) - \boldsymbol{\omega}\cdot\left[\nabla\left(\frac{1}{\rho}\nabla\cdot\mathbf{j}_2\right)\right] - \boldsymbol{\zeta}\cdot\left[\nabla\left(\frac{1}{\rho}\right)\times\nabla p\right] + \boldsymbol{\zeta}\cdot\left[\nabla\times\left(\frac{1}{\rho}\nabla\cdot\overline{\overline{\tau}}\right)\right]. \qquad (13)$$

In eq. 13, the first term in the right hand side represents the effect of compressibility, the second term is due to species mass diffusion, the third term is the baroclinic contribution, and the last one represents the viscous effects. Displayed in Fig. 6 are the HN800 layer average (6a) and RMS (6b) budgets. Locally in $x_2/\delta_{\omega,0}$, viscous and species mass flux effects dominate both the average and RMS, with compressibility and baroclinic contributions being minimal and negligible, respectively; this is physically understandable since locally $\boldsymbol{\omega}$ is influenced by the momentum flux and $\boldsymbol{\zeta}$ is related to the species mass flux. This situation is typical for all layers. This means that locally in $x_2/\delta_{\omega,0}$, $\cos(\boldsymbol{\omega},\boldsymbol{\zeta})$ reflects the non-ideality of the mixture, as the term $\propto \alpha_D$ is largest in eq. 7 [6], [10]. However, from the volume integral

$$\int_V \frac{D}{Dt}(\boldsymbol{\omega}\cdot\boldsymbol{\zeta})\,dV = -\int_V (\boldsymbol{\omega}\cdot\boldsymbol{\zeta})(\nabla\cdot\mathbf{u})\,dV, \qquad (14)$$

it is clear that the compressibility is volumetrically the sole feature influencing the variation of $(\omega \cdot \zeta)$. Therefore, if $(\omega \cdot \zeta) < 0$, to increase this product towards the desired 0 (to maximize A), according to eq. 14 it is desirable to have $\nabla \cdot \mathbf{u} > 0$; on the other hand if $(\omega \cdot \zeta) > 0$, to decrease this product towards the desired 0, it is necessary to have again $\nabla \cdot \mathbf{u} > 0$. This means that volumetrically, dilatation acts similar to a 'restoring force', always tending to induce an increase in surface area, as already seen from eq. 10. A consequence of eq. 14 is that if $dV/dt = 0$ (as herein), then $\partial \left(\int_V (\omega \cdot \zeta) \, dV \right) / \partial t = 0$, which makes this integral a time invariant for V.

4 Conclusions

The interest in increasing combustion efficiency through enlargement of the flame area, as well as the desire to control supercritical fluid disintegration in Diesel, gas turbine and liquid rocket engines, led to the investigation of area production in supercritical, turbulent fluids. To elucidate the physical mechanisms responsible for area variation, a database of turbulent transitional states obtained from Direct Numerical Simulation of supercritical mixing layers was interrogated; each mixing layer was initially density-stratified. This database encompassed two binary-species systems, and two wavelength initial perturbations for each species system. Surfaces whose area was examined in a coordinate system attached to each surface were those perpendicular to the mass fraction gradient.

The results showed that while locally area may be created or destroyed, on average area is always created. Moreover, area creation is larger in the lighter fluid region; a smaller initial density stratification yields a larger area production; the area creation is uncorrelated with the momentum thickness based Reynolds number at the transitional state; and smaller wavelength initial perturbations lead to enlarged area creation. This last observation represents an initial step towards the control of area production.

An examination of the two phenomena responsible for changes in area reveals that in all situations the strain related contribution is substantially larger than that of compressibility, and that this larger term is most active in regions of high density gradient magnitude identified in previous studies of supercritical mixing layers. The preponderant influence of the strain related term motivated the development of the conservation equation for the strain-rate/conserved-scalar-gradient tensorial product, and the examination of its budget. For all layers, strain and convection effects lead to production of area, whereas rotational and

species mass flux effects destroy it; while viscous effects are negligible, pressure gradient effects can either produce or destroy area. Strong pressure-gradient-related RMS were found for the species-system that shows considerable departures from perfect gas and ideal mixture behavior, and were shown to be the manifestation of the strong pressure/density coupling through the equation of state.

To further investigate the reasons for area production, the PDF of the cosine of the vorticity and mass-fraction-gradient vectors was calculated and examined. For all layers the PDFs exhibit a large peak for perpendicular vectors, with the largest peak occurring for the layer displaying the largest area production. This is consistent with the physical picture of orthogonal vorticity and mass-fraction-gradient portraying flames being wrapped around a vortex tube, thereby promoting a larger area. From a derived conservation equation for the vorticity/mass-fraction-gradient scalar product, it is shown that locally in the cross-stream direction, viscous and species mass flux effects dominate both the average and RMS, with compressibility and baroclinic contributions being minimal and negligible, respectively. Since the species mass flux is dominated by mixture non-ideality effects [6], the local area creation is directly related to thermodynamic effects through the equation of state. However, volumetrically, compressibility is the sole phenomenon responsible for the evolution of this scalar product, and it was shown that dilatation acts akin to a restoring force, always tending to lead the system to increased area production. Moreover, the volume integral of this scalar product was found to be a time invariant of the system.

The findings regarding the manifestations of mixture non-ideality and pressure-to-density coupling in determining the area production highlight the importance of real gas thermodynamics in the modeling of supercritical turbulent reactive/non-reactive flows.

ACKNOWLEDGMENT

-Caltech,

This study was conducted at the Jet Propulsion Laboratory, jointly sponsored by the NASA Marshall Space Flight Center with Dr. John Hutt as contract monitor, the Air Force Office of Scientific Research under the direction of Dr. Julian Tishkoff and by the Army Research Office under the direction of Dr. David Mann, under an interagency agreement with NASA. One of the authors (JB) would like to thank Prof. Dale Pullin of the California Institute of Technology for bringing Ref. 1 to her attention, and Mr. E. W. Christiansen and Prof. C. K. Law of Princeton University for graciously providing results on the oxygen/hydrogen flammability limits. Computational resources were provided by the supercomputing facility at JPL.

References

[1] Reutsch, G. R. and Ferziger, J. H., *Annual Research Briefs*, Center for Turbulence Research, Stanford University, 213 (1997)

[2] Matalon, M., Comb. Sci. Techn. 31:169 (1983)

[3] Chung, S. H. and Law, C. K., Comb. Flame 55:123 (1984)

[4] Candel, S. M. and Poinsot, T. J., Combust. Sci. Tech. 70:1 (1990)

[5] Ashurst, W. T., Kerstein, A. R., Kerr, R. M. and Gibson, C. H., Phys. Fluids. 30(8):2343 (1987)

[6] Okong'o, N. and Bellan, J., Direct numerical simulation of a transitional supercritical mixing layer: heptane and nitrogen, submitted to J Fluid Mech., 2000

[7] Okong'o, N. and Bellan, J., Linear stability analysis of real gas two- and three-dimensional mixing layers, submitted to Phys. Fluids, 2001

[8] Bellan, J., Progress in Energy and Combustion Science 26(4-6):329 (2000)

[9] Okong'o, N. and Bellan, J., Characteristics of Supercritical Transitional Temporal Mixing Layers, *IUTAM Symposium on Turbulent Mixing and Combustion*, Kingston, Ontario, in press (2001)

[10] Okong'o, N., Harstad, K and Bellan, J., Direct Numerical Simulations of O_2/H_2 Temporal Mixing Layers under Supercritical Conditions, accepted for publication in the AIAA J., 2001

[11] Harstad, K. and Bellan, J., Combust. Flame, 127(1/2): 1861 (2001)

[12] Harstad, K. and Bellan, J., Int. J. of Multiphase Flow 26(10):1675 (2000)

[13] Nomura, H., Ujiie, Y., Rath, H. J., Sato, J. and Kono, M., Proc. Comb. Inst. 26:1267 (1996).

[14] Miller, R. S., Harstad, K. and J. Bellan, J., J. Fluid Mech. 436:1 (2001)

[15] Sarman, S. and Evans, D. J., Phys. Rev. A45(4):2370 (1992).

[16] Harstad, K. and Bellan, J., Int. J. Heat Mass Transfer 41:3537 (1998)

[17] Moser, R. D. and Rogers, M. M., Phys. Fluids A 3(5):1128 (1991)

[18] Harstad, K. and Bellan, J., Pressure effects on heptane drops in a multicomponent environment, to be submitted for publication, 2001

[19] Christiansen, E. W. and Law, C. K., personal communication, 2001

Case	Heavier/ lighter fluid	$\frac{\lambda_1}{\delta_{\omega,0}}$	F_{3D}	Re_0	Re_m
HN500	C_7H_{16}/N_2	7.29	0.05	500	1250
HN800	C_7H_{16}/N_2	4.57	0.05	800	1256
OH550	O_2/H_2	10.35	0.025	550	1513
OH750	O_2/H_2	7.29	0.05	750	1507

Table 1: Initial conditions of the simulations and value of the momentum thickness based Reynolds number, Re_m, at transition. In all simulations, M_0=0.4, $\delta_{\omega,0}$=6.859$\times 10^{-3}$ m and F_{2D}=0.1. For the C_7H_{16}/N_2 layers, ρ_2/ρ_1=12.88, p_r=2.17 (p=60 atm), T_2=600K and T_1=1000K; for the O_2/H_2 layers, ρ_2/ρ_1=24.40, p_r=1.98 (p=100 atm), T_2=400K and T_1=600K.

Figure Captions

Figure 1. $(1/A)\,(dA/dt)$; (a) average and (b) RMS in $(x_1 - x_3)$ planes for all layers listed in Table 1: HN500 (——), HN800 (– – –),OH750 (– · – · –), OH550 (– · · – · · –).

Figure 2. Budget of $(1/A)\,(dA/dt)$; average in $(x_1 - x_3)$ planes for the HN800 layer: $-S_{ij}\zeta_i\zeta_j/\,(\zeta_k\zeta_k)$ $(\delta_{\omega,0}/\Delta U_0)$ (– · – · –), $S_{kk}\,(\delta_{\omega,0}/\Delta U_0)$ (– – –), $\left[-S_{ij}\zeta_i\zeta_j/\,(\zeta_k\zeta_k) + S_{kk}\right]\,(\delta_{\omega,0}/\Delta U_0)$ (——).

Figure 3. Budget of $\left(-\zeta_i\zeta_j S_{ij}\right)$; (a) average and (b) RMS in $(x_1 - x_3)$ planes for the HN800 layer: $2\partial u_k/\partial x_i\zeta_j\zeta_k S_{ij}\ \left(\delta^4_{\omega,0}/\Delta U_0^2\right)$(——), $S_{ik}S_{kj}\zeta_i\zeta_j\ \left(\delta^4_{\omega,0}/\Delta U_0^2\right)$ (–·–·–), $\left(\omega_i\zeta_i\omega_j\zeta_j - \omega_i\omega_i\zeta_j\zeta_j\right)/4\ \left(\delta^4_{\omega,0}/\Delta U_0^2\right)$ (- - -), $\zeta_i\zeta_j\partial/\partial x_i\,(1/\rho\partial p/\partial x_j)\ \left(\delta^4_{\omega,0}/\Delta U_0^2\right)$ (···), $2\zeta_i S_{ij}\partial/\partial x_j\,(1/\rho\partial j_{2k}/\partial x_k)\ \left(\delta^4_{\omega,0}/\Delta U_0^2\right)$ (— — —), $-\zeta_i\zeta_j\partial/\partial x_i\,(1/\rho\partial\tau_{jk}/\partial x_k)$ $\left(\delta^4_{\omega,0}/\Delta U_0^2\right)$ (– · · – · · –).

Figure 4. Budget of $\left(-\zeta_i\zeta_j S_{ij}\right)$; (a) average and (b) RMS in $(x_1 - x_3)$ planes for the OH750 layer: $2\partial u_k/\partial x_i\zeta_j\zeta_k S_{ij}\ \left(\delta^4_{\omega,0}/\Delta U_0^2\right)$(——), $S_{ik}S_{kj}\zeta_i\zeta_j\ \left(\delta^4_{\omega,0}/\Delta U_0^2\right)$ (–·–·–), $\left(\omega_i\zeta_i\omega_j\zeta_j - \omega_i\omega_i\zeta_j\zeta_j\right)/4\ \left(\delta^4_{\omega,0}/\Delta U_0^2\right)$ (- - -), $\zeta_i\zeta_j\partial/\partial x_i\,(1/\rho\partial p/\partial x_j)\ \left(\delta^4_{\omega,0}/\Delta U_0^2\right)$ (···), $2\zeta_i S_{ij}\partial/\partial x_j\,(1/\rho\partial j_{2k}/\partial x_k)\ \left(\delta^4_{\omega,0}/\Delta U_0^2\right)$ (— — —), $-\zeta_i\zeta_j\partial/\partial x_i\,(1/\rho\partial\tau_{jk}/\partial x_k)$ $\left(\delta^4_{\omega,0}/\Delta U_0^2\right)$ (– · · – · · –).

Figure 5. Probability density function of $\cos(\boldsymbol{\omega}\cdot\boldsymbol{\zeta})$ for all layers listed in Table 1: HN500 (——), HN800 (– – –), OH750 (– · – · –), OH550 (– · · – · · –). For HN layers, $0.005 < Y_2 < 0.995$; for OH layers, $0.4113 < Y_2 < 0.9895$. These limits encompass the overwhelming majority of points within the layers.

Figure 6. Budget of $(\boldsymbol{\omega}\cdot\boldsymbol{\zeta})$; (a) average and (b) RMS in $(x_1 - x_3)$ planes for the HN800 layer: $-\,(\boldsymbol{\omega}\cdot\boldsymbol{\zeta})\,(\nabla\cdot\mathbf{u})$ $\left(\delta^3_{\omega,0}/\Delta U_0^2\right)$ (– · · – · · –), $-\boldsymbol{\omega}\cdot[\nabla\,(1/\rho\nabla\cdot\mathbf{j}_2)]\ \left(\delta^3_{\omega,0}/\Delta U_0^2\right)$ (– · – · –), $-\boldsymbol{\zeta}\cdot[\nabla\,(1/\rho)\times\nabla p]\ \left(\delta^3_{\omega,0}/\Delta U_0^2\right)$ (– – –), $\boldsymbol{\zeta}\cdot\left[\nabla\times\left(1/\rho\nabla\cdot\overline{\overline{\tau}}\right)\right]\ \left(\delta^3_{\omega,0}/\Delta U_0^2\right)$ (——).

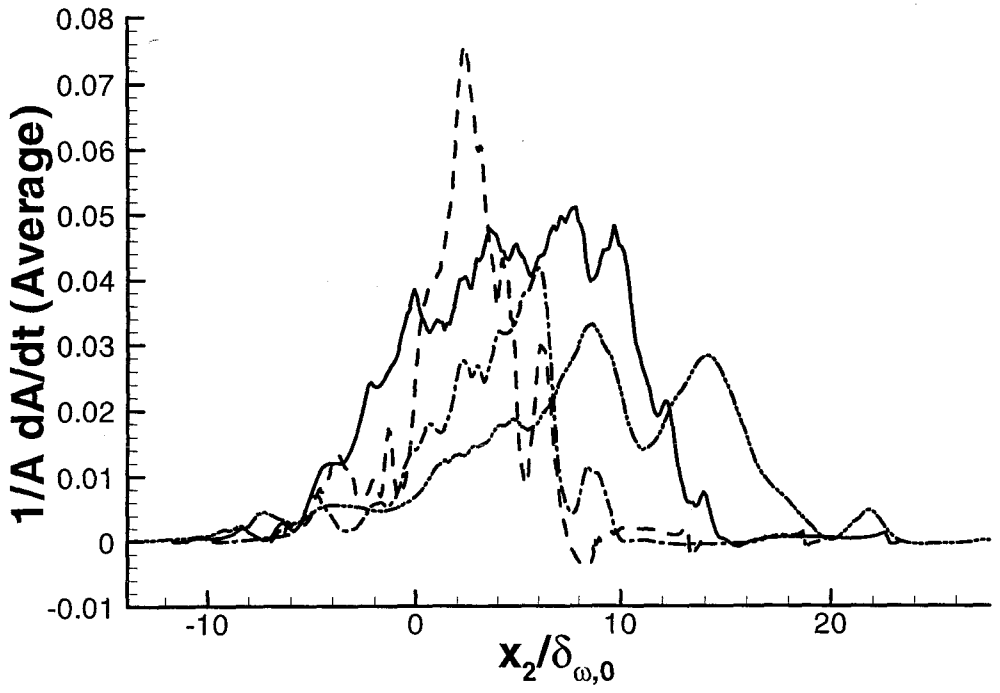

a)

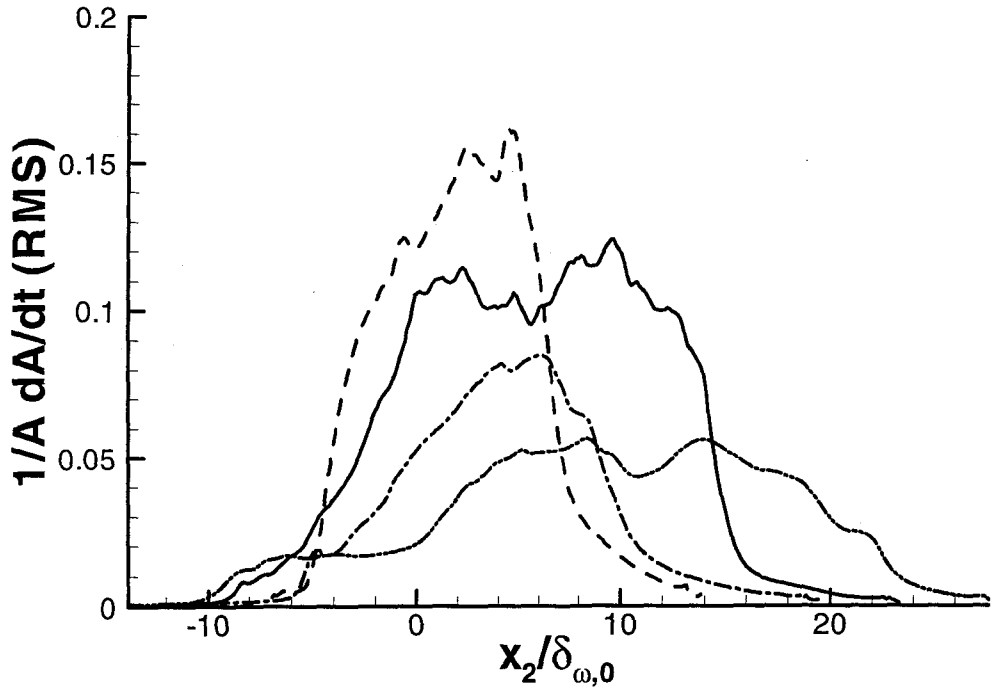

b)

Figure 1: $(1/A)\,(dA/dt)$; (a) average and (b) RMS in $(x_1 - x_3)$ planes for all layers listed in Table 1: HN500 (——), HN800 (– – –),OH750 (– · – · –), OH550 (– · · – · · –).

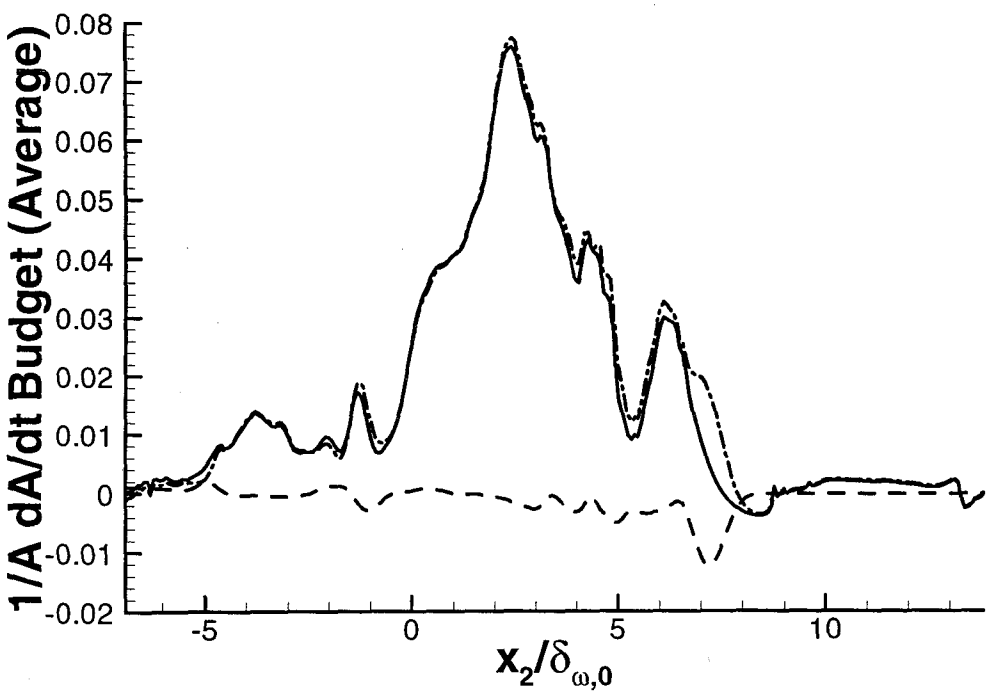

Figure 2: Budget of $(1/A)\,(dA/dt)$; average in $(x_1 - x_3)$ planes for the HN800 layer: $-S_{ij}\zeta_i\zeta_j/\,(\zeta_k\zeta_k)$ $(\delta_{\omega,0}/\Delta U_0)$ $(-\cdot-\cdot-)$, $S_{kk}\,(\delta_{\omega,0}/\Delta U_0)$ $(--)$, $\left[-S_{ij}\zeta_i\zeta_j/\,(\zeta_k\zeta_k) + S_{kk}\right]\,(\delta_{\omega,0}/\Delta U_0)$ (——).

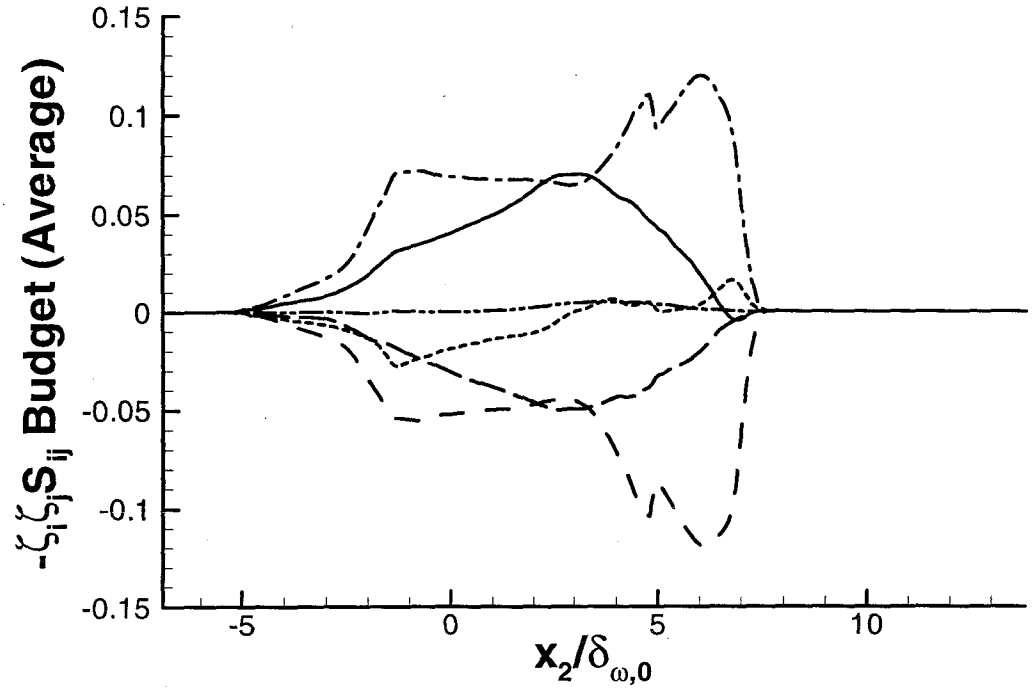

a)

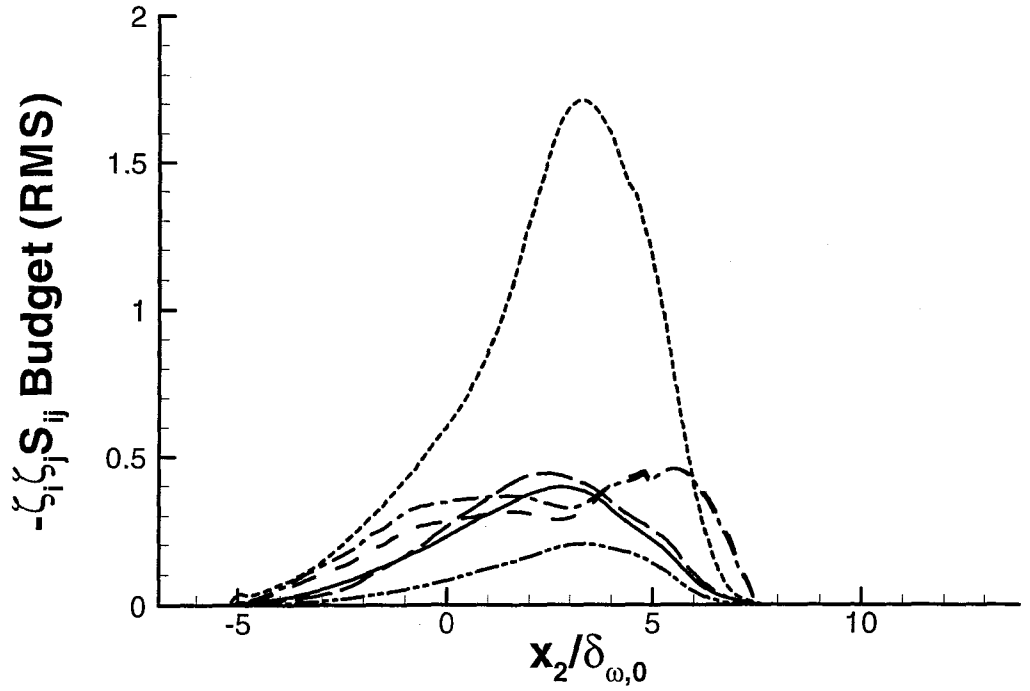

b)

Figure 3: Budget of $(-\zeta_i\zeta_j S_{ij})$; (a) average and (b) RMS in $(x_1 - x_3)$ planes for the HN800 layer: $2\partial u_k/\partial x_i \zeta_j\zeta_k S_{ij}$ $(\delta^4_{\omega,0}/\Delta U_0^2)$(——), $S_{ik}S_{kj}\zeta_i\zeta_j$ $(\delta^4_{\omega,0}/\Delta U_0^2)$ (– · – · –), $(\omega_i\zeta_i\omega_j\zeta_j - \omega_i\omega_i\zeta_j\zeta_j)/4$ $(\delta^4_{\omega,0}/\Delta U_0^2)$ (- - -), $\zeta_i\zeta_j\partial/\partial x_i\,(1/\rho\partial p/\partial x_j)$ $(\delta^4_{\omega,0}/\Delta U_0^2)$ $(\cdots)$, $2\zeta_i S_{ij}\partial/\partial x_j\,(1/\rho\partial j_{2k}/\partial x_k)$ $(\delta^4_{\omega,0}/\Delta U_0^2)$ (— — —), $-\zeta_i\zeta_j\partial/\partial x_i\,(1/\rho\partial\tau_{jk}/\partial x_k)$ $(\delta^4_{\omega,0}/\Delta U_0^2)$ (– · · – · · –).

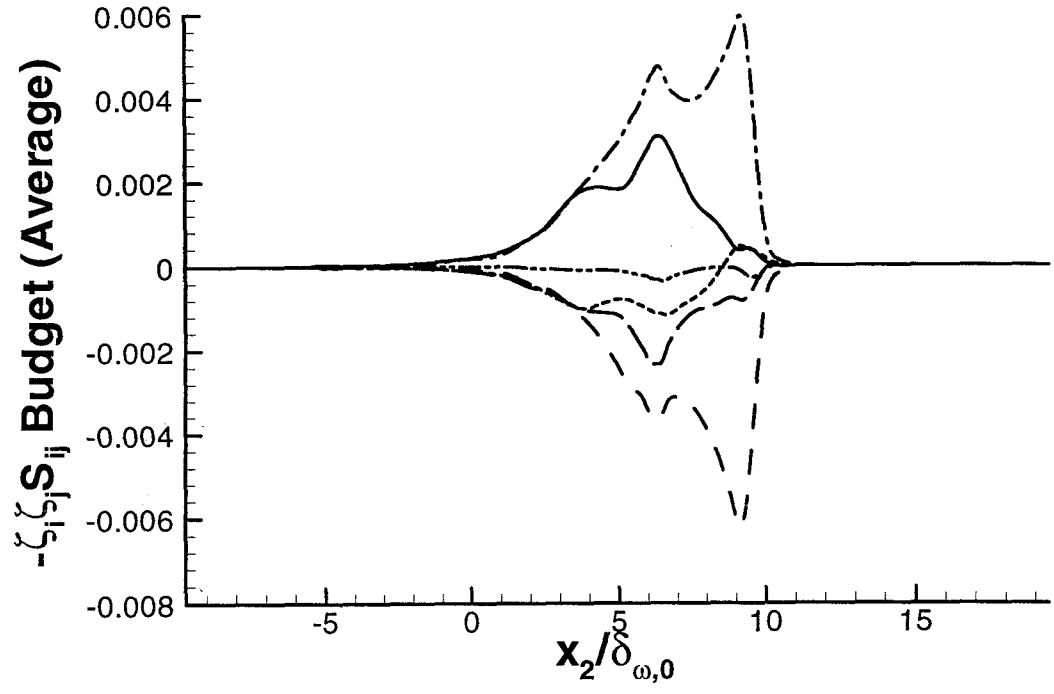

a)

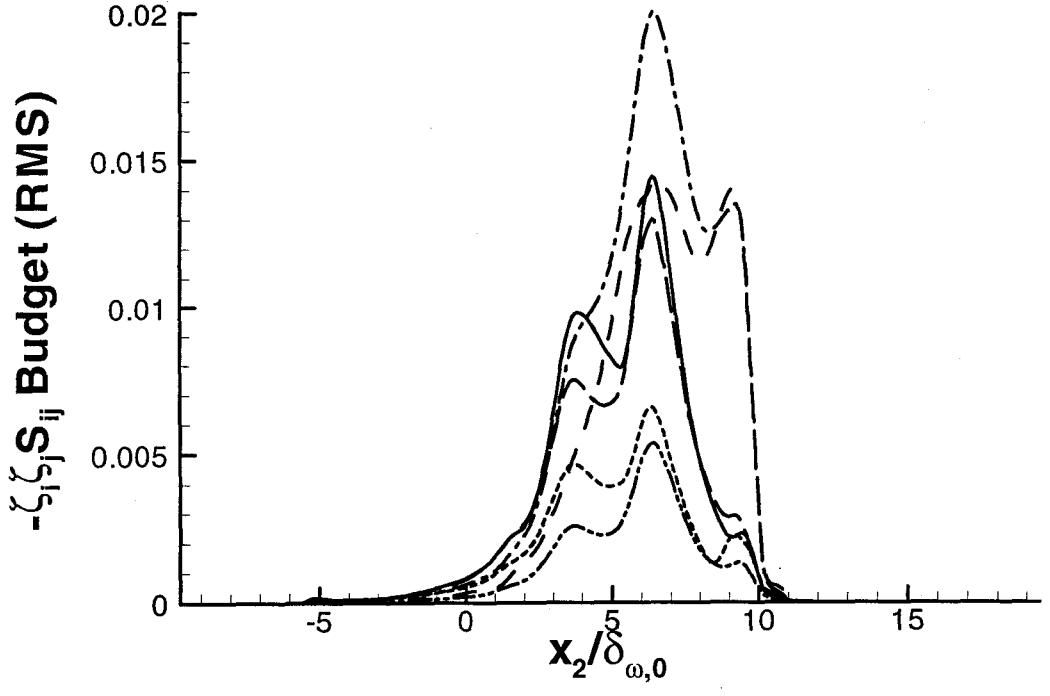

b)

Figure 4: Budget of $(-\zeta_i\zeta_jS_{ij})$; (a) average and (b) RMS in $(x_1 - x_3)$ planes for the OH750 layer: $2\partial u_k/\partial x_i\zeta_j\zeta_kS_{ij}$ $(\delta^4_{\omega,0}/\Delta U_0^2)$(——), $S_{ik}S_{kj}\zeta_i\zeta_j$ $(\delta^4_{\omega,0}/\Delta U_0^2)$ (— · — · —), $(\omega_i\zeta_i\omega_j\zeta_j - \omega_i\omega_i\zeta_j\zeta_j)/4$ $(\delta^4_{\omega,0}/\Delta U_0^2)$ (- - -), $\zeta_i\zeta_j\partial/\partial x_i\,(1/\rho\partial p/\partial x_j)$ $(\delta^4_{\omega,0}/\Delta U_0^2)$ $(\cdots)$, $2\zeta_iS_{ij}\partial/\partial x_j\,(1/\rho\partial j_{2k}/\partial x_k)$ $(\delta^4_{\omega,0}/\Delta U_0^2)$ (— — —), $-\zeta_i\zeta_j\partial/\partial x_i\,(1/\rho\partial\tau_{jk}/\partial x_k)$ $(\delta^4_{\omega,0}/\Delta U_0^2)$ (— · · — · · —).

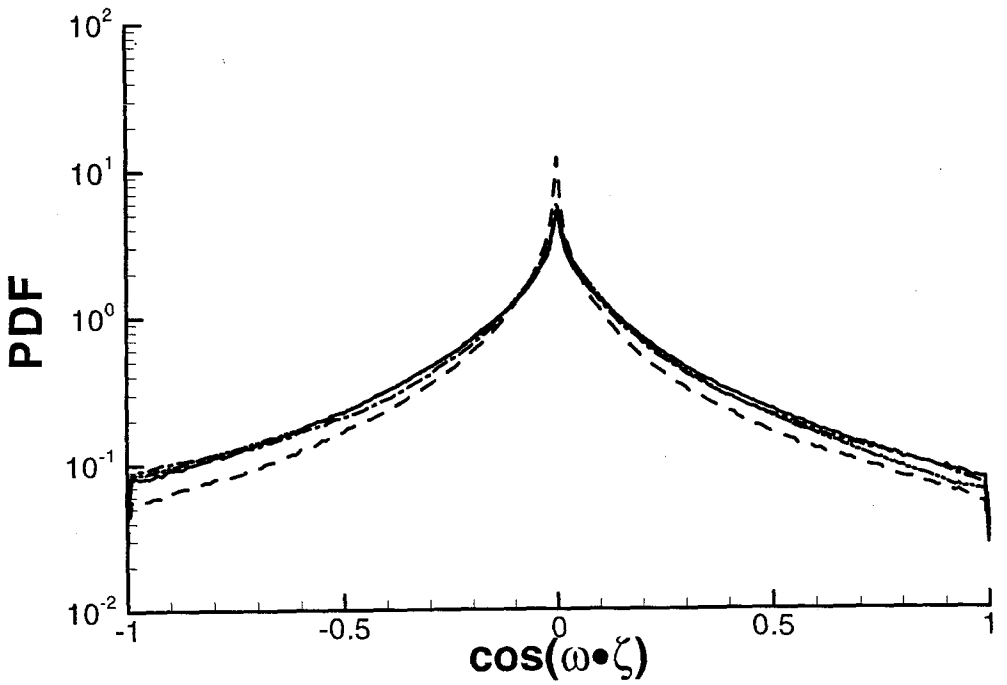

Figure 5: Probability density function of $\cos(\omega \cdot \zeta)$ for all layers listed in Table 1: HN500 (——), HN800 (– – –), OH750 (– · – · –), OH550 (– · · – · · –). For HN layers, 0.005< Y_2 <0.995; for OH layers, 0.4113< Y_2 <0.9895. These limits encompass the overwhelming majority of points within the layers.

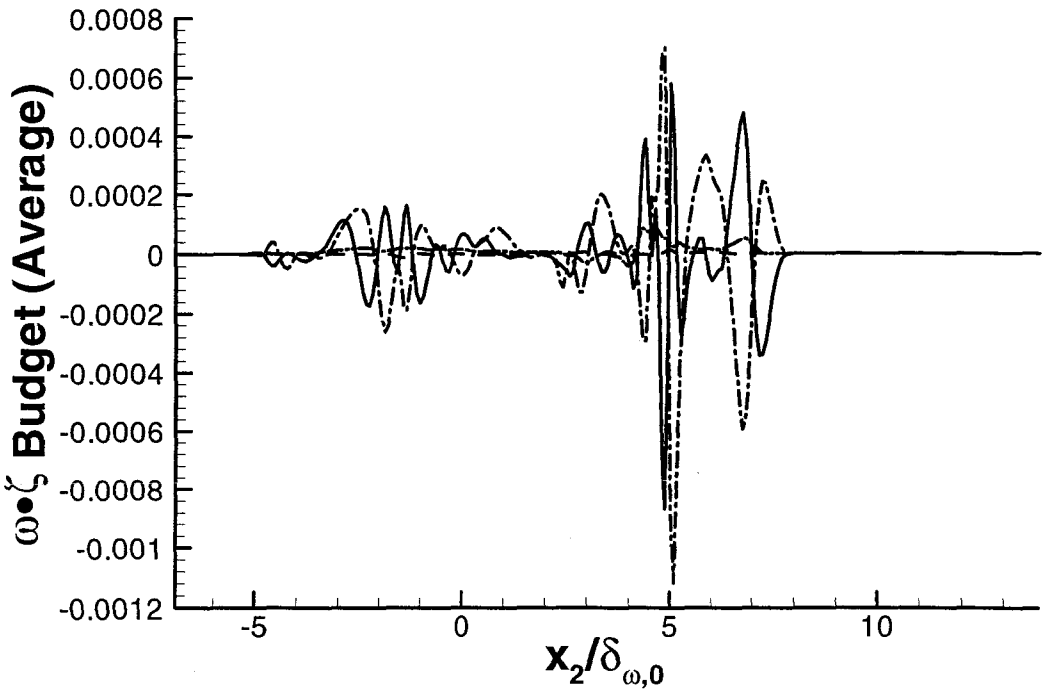

a)

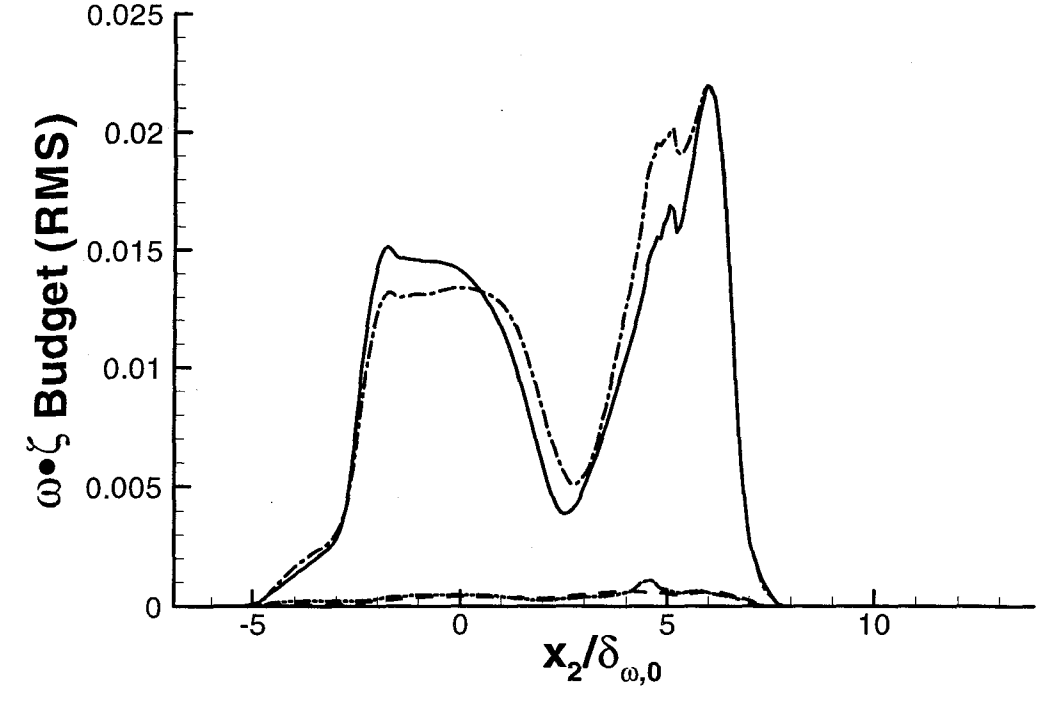

b)

Figure 6: Budget of $(\boldsymbol{\omega}\cdot\boldsymbol{\zeta})$; (a) average and (b) RMS in $(x_1 - x_3)$ planes for the HN800 layer: $-(\boldsymbol{\omega}\cdot\boldsymbol{\zeta})(\nabla\cdot\mathbf{u})$ $\left(\delta^3_{\omega,0}/\Delta U_0^2\right)$ $(-\cdots-\cdots-)$, $-\boldsymbol{\omega}\cdot[\nabla(1/\rho\nabla\cdot\mathbf{j}_2)]$ $\left(\delta^3_{\omega,0}/\Delta U_0^2\right)$ $(-\cdot-\cdot-)$, $-\boldsymbol{\zeta}\cdot[\nabla(1/\rho)\times\nabla p]$ $\left(\delta^3_{\omega,0}/\Delta U_0^2\right)$ $(---)$, $\boldsymbol{\zeta}\cdot\left[\nabla\times(1/\rho\nabla\cdot\overline{\overline{\tau}})\right]$ $\left(\delta^3_{\omega,0}/\Delta U_0^2\right)$ $(——)$.